Chinese Chemical Letters 35 (2024) 108476

Contents lists available at ScienceDirect

Chinese Chemical Letters

journal homepage: www.elsevier.com/locate/cclet

Silicon quantum dots-based fluorescent sensor for the detection of cobalt with high sensitivity and selectivity

Ebtihaj Mohammed Sullam[a,b], Khalid Mohammed Adam[b], Juanjuan Liu[a], Hongli Chen[a,*], Jianxi Xiao[a,*]

[a] State Key Laboratory of Applied Organic Chemistry, College of Chemistry and Chemical Engineering, Lanzhou University, Lanzhou 730000, China
[b] Department of Chemistry, Faculty of Education, University of Kordofan, El Obeid 51111, Sudan

ARTICLE INFO

Article history:
Received 23 November 2022
Revised 2 April 2023
Accepted 17 April 2023
Available online 21 April 2023

Keywords:
Silicon quantum dots
Fluorescence
Poly(vinylpyrrolidine)
Test paper
Cobalt detection

ABSTRACT

Fluorescent silicon quantum dots (Si QDs) were hydrothermally synthesized from a mixture of 3(2-aminoethylamino) propyl (dimethoxymethylsilane) (AEAPDMMS) and poly(vinylpyrrolidine) (PVP). The resulting Si QDs exhibited good water solubility and high stability. Under the optimized conditions, the probe revealed an excellent linear fluorescence quenching effect on Co^{2+} ranging from 1 μmol/L to 120 μmol/L with a limit of detection of 0.37 μmol/L (based on 3 s/*k*). The quenching mechanism was studied, showing that static quenching (SQE) causes the main effect. Furthermore, the test paper based on Si QDs was prepared, which is cost-effective, high sensitivity, good selectivity, easy to use and show excellent anti-interference capability. This method was applied to analyze the content of Co^{2+} in environmental water samples with satisfying results.

Heavy metals found in groundwater are difficult to decompose and thus accumulate in living organisms, causing a threat to the environment and human health [1,2]. Cobalt (Co^{2+}) is a physiologically essential mineral, albeit required in very low amounts, which plays an important role in DNA biosynthesis as an essential component of vitamin B12 [3,4]. In particular, cobalt deficiency inhibits erythropoiesis and myelin synthesis and causes anemia and dementia [5–9]. However, excessive cobalt intake can cause asthma, convulsions, bone defects, stomach disorders, vasodilatation, carcinogenesis, paralysis, and heart disease [1,5,10,11]. The World Health Organization (WHO) recommends the maximum limit of cobalt in drinking water is 1.7 μmol/L [12]. Therefore, it is necessary to design and develop an analytical technique characterized by simplicity and selectivity to detect Co^{2+} to preserve human health and the environment's safety [1,13]. To date, the existing methods for determining Co^{2+}, such as liquid chromatography, electrochemical, and atomic absorption spectrometry, have been reported [2,14-16]. Unfortunately, the relatively complex procedures, costly tests, and tedious sample processing limit these analytical methods. Therefore, it is critical to establish a rapid and facile approach to detect Co^{2+} under low concentrations.

Recently, various fluorescent nanomaterials have been utilized as nanoprobes for Co^{2+} detection with high selectivity and sensitivity. For instance, MTPT-capped CdS QDs was developed for Co^{2+} fluorescence analysis [17]. Some single element-based dots, including carbon [18], phosphorus [19], and sulfur QDs [1] were also used for Co^{2+} detection. Moreover, functionalized carbon dots [20], nitrogen and sulfur co-doped graphene quantum dots [21], and carbon dots prepared using flax straw as carbon source [6] were developed to sense Co^{2+}. However, these fluorometric chemosensors had some inherent issues, such as the weak water solubility, potential toxicity and low sensitivity, may hinder their actual applications. Therefore, searching for more effective materials for fluorometric detection of Co^{2+} with high sensitivity, superior selectivity, outstanding visual ability and excellent portability is important and urgent.

Interestingly, among various detection methods, fluorescent silicon (Si) QDs sensing to detect Co^{2+} exhibits some advantages over other technologies, such as simplicity, high sensitivity, short response time, low instrumentation cost and nontoxic. Further, it can provide and facilitate the naked-eye detection in an uncomplicated manner. Additionally, the sensitivity and selectivity are dependent on the affinity between the active groups on the surface of the Si QDs and the target metal ion [22–24]. Moreover, Si QDs smaller than 10 nm are promising fluorescent nanomaterials with environmental friendliness, high photostability, and remarkable biocompatibility, which have received extensive attentions in multiplex

* Corresponding authors.
E-mail addresses: hlchen@lzu.edu.cn (H. Chen), xiaojx@lzu.edu.cn (J. Xiao).

https://doi.org/10.1016/j.cclet.2023.108476
1001-8417/

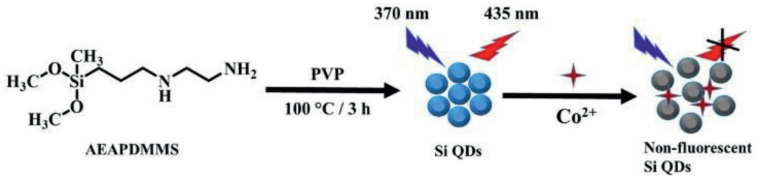

Scheme 1. Schematic representation of hydrothermal preparation of novel fluorescent silicon quantum dots for Co^{2+} detection.

sensing, drug delivery, disease diagnosis, bioimaging and other fields [25–28]. Extensive industry knowledge and investment in silicon-based technologies make it an ideal replacement for other quantum dot materials [29,30].

In this work, Si QDs have been synthesized by a one-step hydrothermal method using polyvinylpyrrolidone (PVP) and 3(2-aminoethylamino) propyl (dimethoxymethylsilane) (AEAPDMMS) as the reductant and silicon source, respectively. Under excited at 370 nm, the synthesized Si QDs exhibited a bright blue fluorescence. The fabrication of the fluorescent sensing platform was characterized by good thermal and optical stability and water solubility based on the prepared Si QDs. It is found that the FL intensity of Si QDs was rapidly and selectively quenched with Co^{2+} addition (Scheme 1). The proposed fluorescent method was successfully applied for detecting Co^{2+} in water samples with satisfactory results. Further, a visual method has been developed by the test paper based on Si QDs, which is fast, economical, and showing excellent anti-interference capability.

As illustrated in Scheme 1, AEAPDMMS was chosen as Si source and PVP as reducing reagent in this work. By using a one-step hydrothermal method, Si QDs were obtained *via* mixing AEAPDMMS and PVP and stirring in an oil bath. In this process, AEAPDMMS to PVP ratio, reaction temperature and time are the important parameters on the fluorescence (FL) intensity. As shown in Figs. S1A and B (Supporting information), the FL intensity was highest as reaction in a row for 2 h at 100 °C. Furthermore, the amount of PVP was optimized with the volume of AEAPDMMS fixed at 1.0 mL. As presented in Fig. S1C (Supporting information), the FL intensity increased with increasing the amount of PVP up to 1 g and then decreased slightly. Therefore, the optimal parameters are as follows: reaction time of 2 h, reaction temperature of 100 °C and AEAPDMMS/PVP ratio of 1.0 mL/1.0 g.

The morphology of the as-synthesized Si QDs was shown in TEM image (Fig. S2A in Supporting information), which appeared spherical with good mono-dispersibility ranging from 2.5 nm to 7.3 nm, while the medial diameter was around 4.1 nm (Fig. S2B in Supporting information). Fig. S3 (Supporting information) presented the FT-IR spectrum of Si QDs. The peaks at 1020 and 934 cm^{-1} were assigned to Si–C and Si–O stretching vibrations, respectively [31]. The signal at 742 cm^{-1} was pertained to the wagging vibration of secondary amine N–H [27,32,33]. The unsaturated bending vibration and stretching vibration absorption peaks at 2950 and 1465 cm^{-1} belonged to the C–H bond [33,34]. The FT-IR spectrum of Si QDs clarified broad N–H and O–H stretching peaks at 3445 cm^{-1} [35,36], indicating that the surface of Si QDs is mostly plated with amino and hydroxyl groups, which means Si QDs have excellent water solubility. Furthermore, the other peaks can be attributed to the stretching vibration of the C=O bond at 1677 cm^{-1} [31] and the C–N bond at 1289 cm^{-1} [37].

XPS spectra illustrated the chemical bonding and surface constitutes of the Si QDs (Fig. 1). The five significant peaks at 102.98, 152.87, 284.05, 399.80 and 531.20 eV are assigned to Si 2p, Si 2s, C 1s, N 1s and O 1s, respectively (Fig. 1A) [33]. Furthermore, four peaks are observed at 284.35 eV, 284.94 eV, 285.77 eV, and 287.56 eV in the C 1s spectrum (Fig. 1B), indicating the presence of C–Si, C–C/C=C, C–N and C=O bonds on the surface of Si QDs

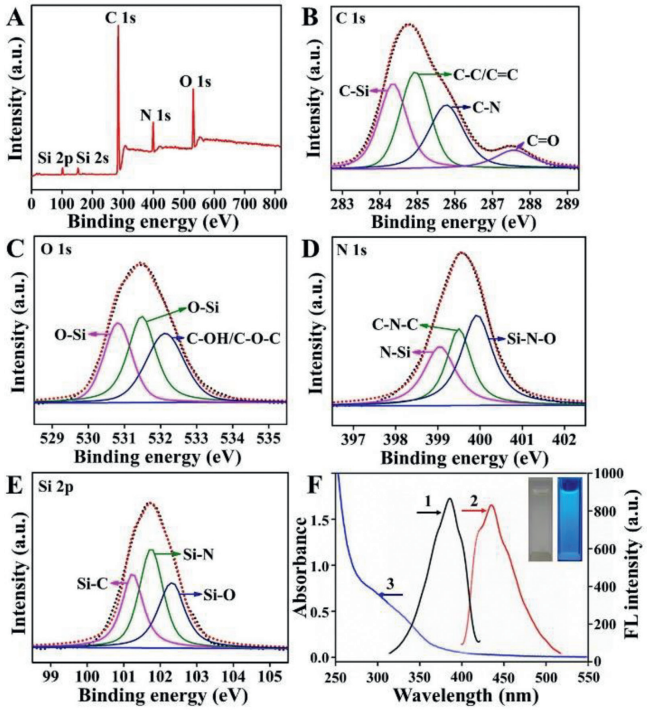

Fig. 1. High resolution XPS spectra of Si QDs: (A) Full range, (B) C 1s, (C) O 1s, (D) N 1s and (E) Si 2p, respectively. (F) FL excitation (1) and emission (2) spectra and UV–vis absorption spectrum (3) of Si QDs, the inset photographs are Si QDs solutions under visible light and UV light illumination.

[36]. Meanwhile, the O 1s spectrum (Fig. 1C) shows three peaks at 530.82 eV, 531.48 eV, and 532.13 eV, which can be assigned to Si–O and C–OH/C–O–C groups, respectively [32,38,39]. The peaks at 399.05 eV, 399.50 eV and 400.00 eV in the high-resolution N 1s spectrum (Fig. 1D) indicate that nitrogen exists mainly in the form of N–Si, C–N–C and Si–N–O groups [40]. High-resolution Si 2p XPS spectrum of the Si QDs (Fig. 1E) show three peaks centered at 101.24 eV, 101.75 eV, and 102.30 eV, which could be belonged to the Si–C, Si–N, and Si–O, respectively [34]. Besides, the optical properties of the Si QDs were confirmed by UV–vis absorption and fluorescence spectra (Fig. 1F). As shown in Fig. 1F, the typical absorption bands appeared at about 285 nm and 342 nm corresponding to the π-π^* transition for C=C and n-π^* transition for C=O or C–N, respectively [41,42]. And the aqueous solution of Si QDs emitted bright blue fluorescence under UV light (365 nm) and colorless under sunlight. From Fig. S4 (Supporting information), 370 nm was adopted as the optimum excitation wavelength for the further experiments due to the strongest fluorescent emission at 435 nm. The synthesized Si QDs showed absolute quantum yield 2.36% obtained by Edinburgh FLS920. The above results strongly support that the N–H and O–H functional groups are on the surface of Si QDs, guaranteeing the excellent water solubility and enhancing the application as luminescent sensors in aqueous solution.

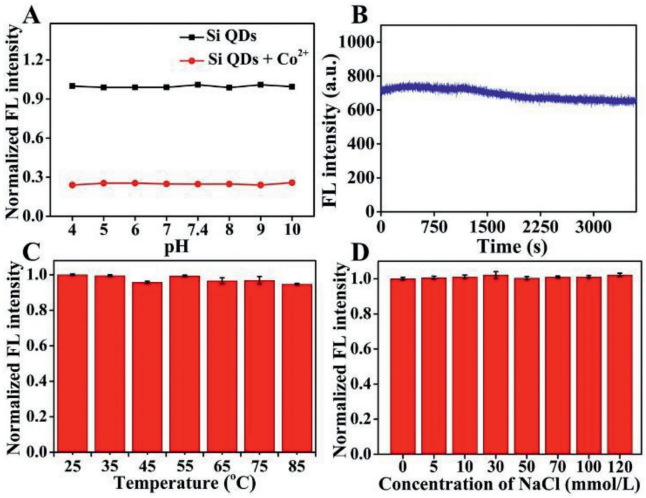

Fig. 2. (A) Influence of pH on the fluorescence spectra of Si QDs in response to Co^{2+} in aqueous buffered solution. (B) FL intensity of Si QDs as function of time. (C) Normalized FL intensity of Si QDs after incubation at different temperature for 4 min. (D) Normalized FL intensity of the Si QDs in 10 mmol/L PBS (pH 7.4) with different concentrations of NaCl. Error bars stand for the standard deviation of three independent experiment. $\lambda_{ex} = 370$ nm, $\lambda_{em} = 435$ nm.

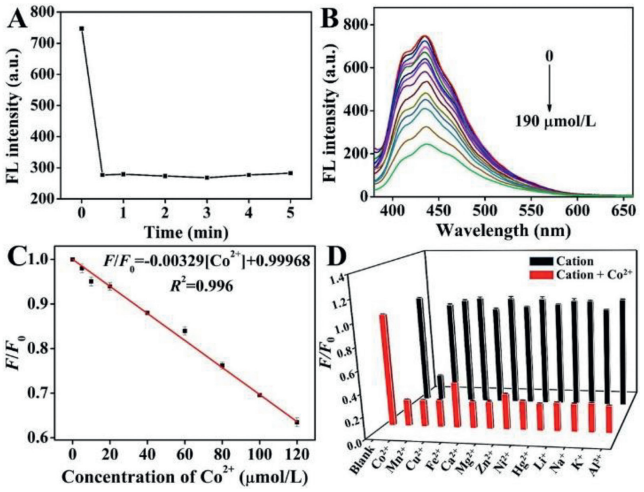

Fig. 3. (A) Time-dependent interaction between Si QDs and Co^{2+} (190 μmol/L) at room temperature. (B) Fluorescence intensity of Si QDs upon addition of various concentrations of Co^{2+} (from top to bottom, 0, 1, 5, 10, 20, 40, 60, 80, 100, 120, 150, 170, 180 and 190 μmol/L respectively) in 10 mmol/L PBS solution (pH 7.4). (C) Calibration curve for Si QDs with increasing concentration of Co^{2+} (1–120 μmol/L). (D) F/F_0 response of the Si QDs to other kinds of cations (380 μmol/L) in the absence (black bars) or presence (red bars) of 190 μmol/L Co^{2+}. $\lambda_{ex} = 370$ nm. Error bars stand for the standard deviation of three independent experiments.

The stability investigation of Si QDs is significant for its wide application. As shown in Fig. 2A, the fluorescence activities were stable with pH ranging from 4 to 10, indicating that the solution acidity did not influence the fluorescence intensity of Si QDs, and the Si QDs sensor could efficiently detect Co^{2+} in a wide pH range. As shown in Fig. 2B, it appeared utterly stable after exposing the Si QDs sensor to light illumination for one hour. Moreover, when the temperature increased from 25 °C to 85 °C, the FL intensity of the Si QDs remained unchanged (Fig. 2C). The stability of Si QDs was also assessed in an ionic medium, where the fluorescence intensity of the Si QDs remained the same in the concentrations range of NaCl from 0 to 120 mmol/L (Fig. 2D). Therefore, the sensor Si QDs showed high stability, and could be used in different practical applications.

The response time of the fluorescent sensing was investigated. As shown in Fig. 3A, when the Si QDs and Co^{2+} solutions were mixed, the fluorescence quenched very fast and reached a plateau within 30 s, indicating that the probe can detect Co^{2+} quickly. Fig. 3B shows the fluorescence spectra of Si QDs in the presence of different concentrations of Co^{2+} in PBS buffer solution (pH 7.4). As illustrated in Fig. 3B, the bright blue fluorescence emitted from the Si QDs solution can be effectively quenched with an increasing concentration of Co^{2+}. Further, as seen in Fig. S5 (Supporting information), there is a continuous shift trend in the CIE coordinates from (0.159, 0.104) to (0.165, 0.128) in the blue gamut with the increase of Co^{2+} concentration, verifying the corresponding fluorescence color changes. Fig. 3C shows the quenching efficiency (F/F_0) has an excellent linear relationship with Co^{2+} concentration in the range of 1–120 μmol/L ($R^2 = 0.996$) with a limit of detection (LOD) of 0.37 μmol/L (based on 3 s/k, where s is the standard deviation of the blank solution and k is the slope of the calibration curve). Although Si QDs show a moderate linear range and sensitivity for Co^{2+} detection compared with some previous Co^{2+} probes (Table S1 in Supporting information), they are easy to fabricate and have advantages in comprehensive ability.

High selectivity for analytes from potentially competing species is an important feature of probes. To explore the selectivity of Si QDs for Co^{2+}, the effects of cations (Na^+, K^+, Li^+, Ca^{2+}, Mg^{2+}, Mn^{2+}, Ni^{2+}, Zn^{2+}, Hg^{2+}, Cu^{2+}, Fe^{2+} and Al^{3+}), anions (F^-, Cl^-, Br^-, I^-, CN^-, SCN^-, ClO_4^-, HSO_4^-, CO_3^{2-}, and $H_2PO_4^-$), and some molecules (catechol, glutathione, methionine, glucose, cysteine, hydroquinone, histidine, valine and arginine) were investigated. The emitted fluorescence of Si QDs solution was quenched upon addition of Co^{2+} (190 μmol/L) (Fig. 3D, Fig. S6 in Supporting information). However, upon addition of interfering metal ions, the F/F_0 ratio (F and F_0 are fluorescence intensities of Si QDs in the presence and absence of the target, respectively) is approximately close to 1, indicating a selective response of Si QDs to Co^{2+}. Moreover, the anti-interference performance of the sensing system was also evaluated, as shown in Fig. 3D and Fig. S7 (Supporting information); Si QDs did not show a significant fluorescence response to any interference other than Co^{2+}. These results indicate that the detection system has excellent selectivity and a strong tolerance to Co^{2+}.

To investigate the fast, convenient and economical detection of Co^{2+}, a facile and visual method was developed by Si QDs-based test paper. Under UV irradiation of 365 nm, the entire test paper showed bright-blue fluorescence (Fig. 4A-a). A series of test papers based on Si QDs for different concentrations of Co^{2+} from 0 to 80 μmol/L were displayed in Fig. 4A-b. The fluorescence of the Si QDs paper sensor was quenched under the UV lamp and the color changes could be easily distinguished with naked eyes related to those concentrations of Co^{2+}. The selectivity of paper sensor was also tested for the detection of various other ions (*i.e.*, Al^{3+}, Fe^{2+}, Cu^{2+}, Hg^{2+}, Mn^{2+}, Mg^{2+}, Zn^{2+}, Ca^{2+}, Ni^{2+}, Li^+, Na^+, K^+, F^-, Cl^-, Br^-, I^-, CN^-, SCN^-, ClO_4^-, HSO_4^-, CO_3^{2-}, $H_2PO_4^-$) under the same conditions (Fig. S8 in Supporting information). As shown in Fig. 4A-c, no obvious fluorescence quenching was observed in the presence of other interfering metal ions. Meanwhile, the anti-interference performance of the paper sensor was also evaluated by dipping a mixture consisting of other 12 metal ions and Co^{2+} with different concentrations into the sensing system. A remarkable fluorescence quenching appeared with the increase of Co^{2+} concentration (Fig. 4A-d), which was basically consistent with the result in the absence of the interfering ions (Fig. 4A-b).

In addition, three-dimensional (3D) models of the corresponding responsive field were used to obtain quantitative fluorescence intensity by ImageJ software (Fig. 4B), reflecting the color change of the test paper more intuitively. Moreover, it was seen that each chromaticity was uniform over a whole piece of test paper due to

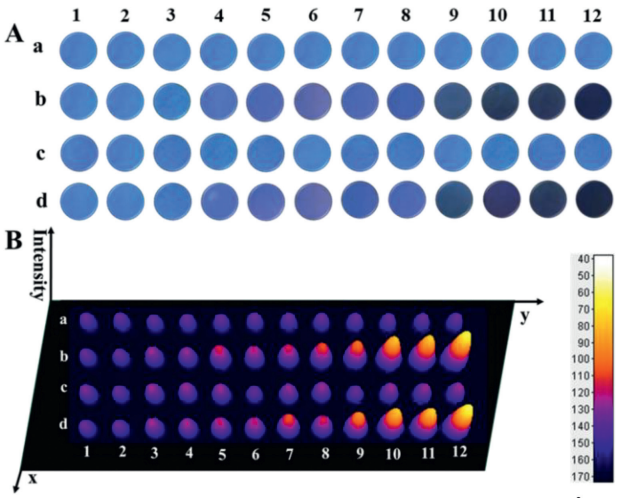

Fig. 4. The Si QDs-based paper sensor for visual detection of Co^{2+}. (A) Photographs of test paper staining with the Si QDs under UV irradiation of 365 nm: (a) only Si QDs; (b) with different concentrations of Co^{2+} (from 1 to 12 are 0.1, 0.5, 1, 5, 10, 20, 30, 40, 50, 60, 70 and 80 μmol/L); (c) with different interfering metal ions (80 μmol/L, from 1 to 12: Na^+, K^+ Li^+, Ca^{2+}, Mg^{2+}, Mn^{2+}, Ni^{2+}, Zn^{2+}, Hg^{2+}, Cu^{2+}, Fe^{2+} and Al^{3+}); (d) with the mixture of other 12 interfering metal ions (80 μmol/L) and Co^{2+} with different concentrations (from 1 to 12 are 0.1, 0.5, 1, 5, 10, 20, 30, 40, 50, 60, 70 and 80 μmol/L). (B) The 3D models of the images in part A.

Table 1
Detection of Co^{2+} in environmental water samples.

Sample	Spiked amount (μmol/L)	Found amount (μmol/L)	Recovery (%)	RSD (%, $n = 3$)
Yellow River sample	10.00	10.20	102.0	3.1
	20.00	19.80	99.0	2.9
	30.00	30.90	103.0	2.7
Tap water sample	10.00	9.87	98.7	1.7
	20.00	20.20	101.0	3.4
	30.00	29.36	97.9	2.8

the homogeneous distribution. Significantly, the chromatic density of the test paper gradually increased with the increasing cobalt concentration, and it appeared deepest at 80 μmol/L. The bright-blue test paper exhibited a dosage-sensitive color response with a discernable scale as low as 1 μmol/L with the observation of naked eye.

To evaluate the feasibility and reliability of this proposed method, the probe Si QDs was applied to determine Co^{2+} in Yellow River water and tap water samples. The emission spectrum for Co^{2+} determination was recorded at an excitation wavelength of 370 nm. Standard additional methods were used to verify the accuracy of the method, and the recoveries were determined by adding 10, 20 and 30 μmol/L Co^{2+}. As shown in Table 1 and Fig. S9 in Supporting information, the average recoveries of Co^{2+} reached 97.9%–103%.

Thus, the accuracy and precision of this proposed approach are satisfactory, indicating that the probe can be applied to detect Co^{2+} in environmental water samples. Moreover, the Si QDs-based test paper was applied to the detection of Co^{2+} in river water and tap water samples (Fig. S10 in Supporting information), indicating it is a simple and economical sensing platform for rapid and visual determination of Co^{2+}.

Fluorescence quenching can be from fluorescence resonance energy transfer (FRET) or inner filter effect (IFE) when there is an overlap between the luminescent substance's emission or excitation spectra and the quencher's UV–vis absorption spectrum [43,44]. In our work, there is no noticeable overlap between the absorption spectrum of Co^{2+} and the FL excitation/emission spectra of Si QDs (Fig. 5A), meaning no FRET or IFE mechanism. Static quenching effect (SQE) or dynamic quenching effect (DQE) is also an important mechanism of FL quenching. Generally, for SQE, a stable compound is formed between the fluorophore and other molecules [12]; for DQE, the collision happens between the quencher and the fluorophore during the return of the luminescent substance to the ground state [39]. Furthermore, SQE and DQE fit into the Stern-Volmer equation (Eq. 1) [45].

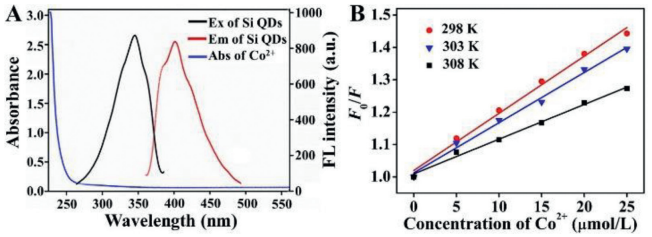

Fig. 5. (A) FL excitation spectrum (black) and emission spectrum (red) of Si QDs, and UV–vis absorption spectrum of Co^{2+} (blue). (B) Stern-Volmer plot of Si QDs solution upon the addition of different concentrations of Co^{2+} (5, 10, 15, 20 and 25 μmol/L).

$$F_0/F = 1 + K_q\tau_0[C] = 1 + K_{sv}[C] \quad (1)$$

where K_q is the FL quenching rate constant which reflects the effects of inter-diffusion and inter-collision in this system. F and F_0 refer to the steady-state FL intensities of the fluorophore in the presence and absence of quencher. K_{sv} is the Stern-Volmer quenching constant. $[C]$ is the concentration of the quencher. τ_0 refers to the average lifetime of the fluorophore in the absence of quencher. Conforming to Eq. 1, K_q values were calculated as 3.40×10^{12}, 2.99×10^{12} and 2.07×10^{12} L mol^{-1} s^{-1}, with their corresponding temperatures at 298, 303 and 308 K (Table S2 in Supporting information). When the plot of F_0/F *versus* $[C]$ in a certain concentration range gives an ascending curvature, the quenching could be assigned to a single static or dynamic [12].

The average FL lifetime of the prepared Si QDs in our work is 5.19 ns (Table S3 in Supporting information). The FL lifetime of Si QDs in the presence of different concentrations of Co^{2+} was studied for an in-depth investigation of which mechanism is responsible for the FL quenching. As observed in Fig. S11 and Table S3 (Supporting information), the FL lifetime of Si QDs did not change in the presence and absence of Co^{2+}. This suggests that the FL of Si QDs was statically quenched by Co^{2+} [46]. Moreover, as observed in Fig. 5B, the linear relationship between Co^{2+} concentrations (5, 10, 15, 20 and 25 μmol/L) and F_0/F is good. In addition, as shown in Table S2 (Supporting information), the K_q and K_{sv} (slope) values decrease with increasing temperature. All K_q values were much larger than the maximum dynamic K_q (2.0×10^{10} L mol^{-1} s^{-1}). Thus, it is further suspected that the quenching is caused by SQE [39]. Not surprisingly, mixing Si QDs and Co^{2+} led to an obvious peak at 350–400 nm appearing in the UV–vis absorption spectra compared to the overlay curve (red dotted curve) in Fig. S12 (Supporting information), illustrating that the affinity and the H-bonding interactions between the active groups on the surface of the Si QDs and Co^{2+} may be responsible for the fluorescence quenching [22]. Therefore, the above results confirm that the FL deletions are mainly caused by SQE rather than DQE [12].

In this work, we have developed a rapid and facile one-pot method to synthesize Si QDs with high stability under a broad range of chemical conditions and described a sensitive and selective Si QDs-based fluorescence method to detect Co^{2+} in an aqueous medium. The detection limit for Co^{2+} was 0.37 μmol/L based on 3σ/slope with a linear range from 1 μmol/L to 120 μmol/L. The static quenching effect is mainly responsible for the fluorescence

quenching of the Si QDs by Co^{2+}. Meanwhile, the high selectivity and sensitivity can ensure Si QDs as a realistic nanoprobe for quantifying Co^{2+} in real water samples with good recoveries. Additionally, we have prepared test papers based on Si QDs, which are cost-effective, easy-to-use and show excellent anti-interference ability, and can detect Co^{2+} in water samples quickly and efficiently.

Declaration of competing interest

The authors declare that they have no known competing financial interests or personal relationships that could have influenced the work reported in this study.

Acknowledgments

The authors are grateful for financial support from the National Natural Science Foundation of China (Nos. 21874060, 22074057 and 21775059).

Supplementary materials

Supplementary material associated with this article can be found, in the online version, at doi:10.1016/j.cclet.2023.108476.

References

[1] L. Li, C. Yang, Y. Li, Y. Nie, X. Tian, J. Mater. Sci. 56 (2021) 4782–4796.
[2] M. Tian, J. Zhang, Y. Liu, Y. Wang, Y. Zhang, Spectrochim. Acta A 252 (2021) 119541.
[3] B. Ke, L. Ma, T. Kang, et al., Anal. Chem. 90 (2018) 4946–4950.
[4] C.G. Fraga, Mol. Aspects Med. 26 (2005) 235–244.
[5] Z. Liu, X. Jia, P. Bian, Z. Ma, Analyst 139 (2014) 585–588.
[6] G. Hu, L. Ge, Y. Li, et al., J. Colloid Interface Sci. 579 (2020) 96–108.
[7] Y. Shiraishi, Y. Matsunaga, T. Hirai, Chem. Commun. 48 (2012) 5485–5487.
[8] M. Gharehbaghi, F. Shemirani, M.D. Farahani, J. Hazard. Mater. 165 (2009) 1049–1055.
[9] A.H. Gore, D.B. Gunjal, M.R. Kokate, et al., ACS Appl. Mater. Interfaces 4 (2012) 5217–5226.
[10] M. Zafer, C.S. Keskin, A. Özdemir, Spectrochim. Acta A 239 (2020) 118487.
[11] S. Ghosh, J.R. Bhamore, N.I. Malek, et al., Spectrochim. Acta 215 (2019) 209–217.
[12] S. Nsanzamahoro, W. Cheng, F.P. Mutuyimana, et al., Talanta 210 (2020) 120636.
[13] S. Geng, S.M. Lin, Y. Shi, et al., Microchim. Acta 184 (2017) 2533–2539.
[14] L. Li, X. Xue, H. Zhang, et al., Chin. Chem. Lett. 32 (2021) 2139–2142.
[15] A. Pramanik, S. Amer, F. Grynszpan, M. Levine, Chem. Commun. 56 (2020) 12126–12129.
[16] L. Meng, Q. Zhu, J.H. Yin, N. Xu, J. Photochem. Photobiol. B: Biol. 173 (2017) 508–513.
[17] F. Faridbod, A. Jamali, M.R. Ganjali, et al., J. Fluoresc. 25 (2015) 613–619.
[18] L. Cao, X. Wang, M.J. Meziani, et al., J. Am. Chem. Soc. 129 (2007) 11318–11319.
[19] X. Zhang, H. Xie, Z. Liu, et al., Angew. Chem. Int. Ed. 54 (2015) 3653–3657.
[20] Y.H. Ng, S.F. Chin, S.C. Pang, S.M. Ng, Sens. Actuators B: Chem. 273 (2018) 83–92.
[21] W. Boonta, C. Talodthaisong, S. Sattayaporn, et al., Mater. Chem. Front. 4 (2020) 507–516.
[22] S.A. El-Safty, Adsorption 15 (2009) 227–239.
[23] K.O. Soetan, C.O. Olaiya, O.E. Oyewole, African J. Food Sci. 4 (2010) 200–222.
[24] X. Wen, G. Wen, W. Li, et al., Mater. Sci. Eng. C 123 (2021) 112022.
[25] L.M.T. Phan, S.H. Baek, T.P. Nguyen, et al., Mater. Sci. Eng. C 93 (2018) 429–436.
[26] A. Noiri, K. Takeda, J. Yoneda, et al., Nano Lett. 20 (2020) 947–952.
[27] X. Li, Z. Zhou, C.C. Zhang, et al., Inorg. Chem. 57 (2018) 8866–8873.
[28] S. Terada, Y. Xin, K. Saitow, Chem. Mater. 32 (2020) 8382–8392.
[29] C. Tu, X. Ma, A. House, S.M. Kauzlarich, A.Y. Louie, ACS Med. Chem. Lett. 2 (2011) 285–288.
[30] C.J.T. Robidillo, J.G.C. Veinot, ACS Appl. Mater. Interfaces 12 (2020) 52251–52270.
[31] Y. Han, Y. Chen, J. Feng, et al., Talanta 194 (2019) 822–829.
[32] S. Nsanzamahoro, W.F. Wang, Y. Zhang, et al., Anal. Chem. 93 (2021) 15412–15419.
[33] Y.Z. Ding, W.F. Wang, T. Chai, et al., Talanta 197 (2019) 113–121.
[34] Y. Liu, Y. Cao, T. Bu, et al., Microchim. Acta 186 (2019) 399.
[35] X. Yuan, B. Wang, C. Yan, et al., Microchem. J. 158 (2020) 105263.
[36] Y. Bai, Q. Su, J. Xiao, F. Feng, X. Yang, Talanta 220 (2020) 121410.
[37] M. Na, Y. Chen, Y. Han, et al., Food Chem. 288 (2019) 248–255.
[38] Z. Fang, Y. Liang, X. Wang, et al., Chin. Chem. Lett. 32 (2021) 2856–2860.
[39] S. Nsanzamahoro, Y. Zhang, W.F. Wang, et al., Microchim. Acta 188 (2021) 46.
[40] X. Geng, Z. Li, Y. Hu, et al., ACS Appl. Mater. Interfaces 10 (2018) 27979–27986.
[41] S. Nsanzamahoro, F.P. Mutuyimana, Y. Han, et al., Sens. Actuators B: Chem. 281 (2019) 849–856.
[42] W. Dong, C. Sun, M. Sun, et al., ACS Appl. Nano Mater. 3 (2020) 312–318.
[43] Y. Han, Y. Chen, J. Feng, et al., Anal. Chem. 89 (2017) 3001–3008.
[44] N. Mahapatra, S. Panja, A. Mandal, M. Halder, J. Mater. Chem. C 2 (2014) 7373–7384.
[45] J. Liu, Y. Chen, L. Wang, et al., J. Agric. Food Chem. 67 (2019) 3826–3836.
[46] F.P. Mutuyimana, J. Liu, S. Nsanzamahoro, et al., Microchim. Acta 186 (2019) 163.